Sheared Wing-Tip Aerodynamics: Wind-Tunnel and Computational Investigation

P. M. H. W. Vijgen*
High Technology Corporation, Hampton, Virginia
C. P. van Dam†
University of California, Davis, California
and
B. J. Holmes‡
NASA Langley Research Center, Hampton, Virginia

Computational and experimental performance benefits are presented for a high-aspect-ratio unswept wing configuration with sheared tips. The sheared tip is a highly swept and highly tapered surface located in the same plane as the inboard wing panel to which it is attached. The computational results were obtained with an inviscid surface panel method that models the nonlinear influence of the trailing wake. Both wind-tunnel and calculated results were obtained for a 12-ft span wing model with various wing-tip configurations. The computational and experimental data are in fair agreement and demonstrate that sheared wing tips can reduce induced drag at cruise and climb lift coefficients. The drag reduction is the result of wake deformation effects and changes in spanwise load distribution. Wind-tunnel measured longitudinal and lateral directional stability characteristics are also presented for the various wing-tip layouts.

Introduction

INDUCED drag is associated with the shedding of vorticity along the span of a finite lifting wing and, in particular, in the wing-tip region. For most subsonic airplane configurations, induced drag contributes nearly 50% of the total drag in optimum cruising flight and contributes much more than 50% of the total drag in climbing flight. Consequently, a strong interest has always existed in the effects of wing planform and wing-tip shape on induced drag.

It is well known that induced drag D_i is a function of the square of the span loading: $D_i \propto (L/b)^2$. The level of induced drag can be decreased by increasing the wing span b for constant lift L. When wing span is constrained, induced-drag reduction can be achieved by improving the aerodynamic efficiency of the wing. Past research efforts have resulted in several successful aerodynamic concepts, including endplates,[1,2] winglets,[3] tip sails,[4,5] and vortex diffusers.[6] The potential gains from these past approaches are limited by wing-root-bending-moment and wetted-area considerations. Also, most of these past approaches were developed based on linear aerodynamic wing theory, which assumes no wake deflection or vortex rollup.

Recent computational results,[7-9] using nonlinear aerodynamic theory, demonstrate the potentially favorable influence of swept or sheared wing tips and crescent wing planforms on the aerodynamic efficiency of lifting surfaces. Sheared tips are both highly swept and highly tapered, and they are located in the same plane as the inboard wing panel to which they are attached. According to classical wing theory, a planar unswept wing of elliptical planform is considered to be the optimum shape for minimum induced drag for a given span loading.[10,11] However, for a given span loading, the induced drag produced by an untwisted planar wing with rearward curvature (also called a crescent or lunate wing planform) can be less than that of the classical optimal wing.[9] The reduction in induced drag results from the nonplanar trailing wake produced by wings with rearward curvature at lifting conditions.

In the present paper, both computational and experimental results are presented which demonstrate the effect of sheared wing tips on wing performance and static-stability characteristics.

Computational Method and Design

The classical wind-tunnel results of Maskell[12] show that immediately downstream of the trailing edge the vortex wake shed from an unswept lifting surface tends to be nearly planar. The trailing vortex wake moves downward under the influence of the bound vortex and under its own influence. Sears[13] proves that, as long as the trailing vortex sheet remains planar, the downward motion of the sheet does not affect induced drag for a given lift. Weston[14] conducted wind-tunnel tests on a swept wing and reports a nonplanar wake effect on induced drag that cannot be explained using linear wing theory (i.e., a vortex-lattice-method with a fixed planar wake model). Unlike the trailing edge of an unswept wing, the geometry of a planar but swept wing becomes nonplanar at angle of attack. For swept wings, the trailing wake thus deforms immediately downstream of the trailing edge, and this is thought to cause the changes in induced drag. Classical wing theory[10,11] does not account for the effects of wake deformation on the lift and drag forces generated by a lifting surface.

The surface-panel method developed by Maskew[15] (VSAERO) models the nonplanar trailing vortex sheet and therefore accounts for the influence of the wake on the aerodynamic forces acting on the wing. The method allows for wake relaxation and wake rollup; a rapidly converging iterative procedure aligns the wake panels with the local flow and provides for the essential nonlinear effect of the three-dimensional wake. Figure 1 depicts a surface panel representation of a

Presented in part as Paper 87-2481 at the AIAA 5th Applied Aerodynamics Conference, Monterey, CA, Aug. 17-19, 1987; received Sept. 30, 1987; revision received Sept. 12, 1988. This paper is declared a work of the U.S. Government and is not subject to copyright protection in the United States.

*Research Engineer. Member AIAA.
†Assistant Professor, Department of Mechanical Engineering, Division of Aeronautical Science and Engineering. Member AIAA.
‡Head, Flight Applications Branch. Associate Fellow AIAA.

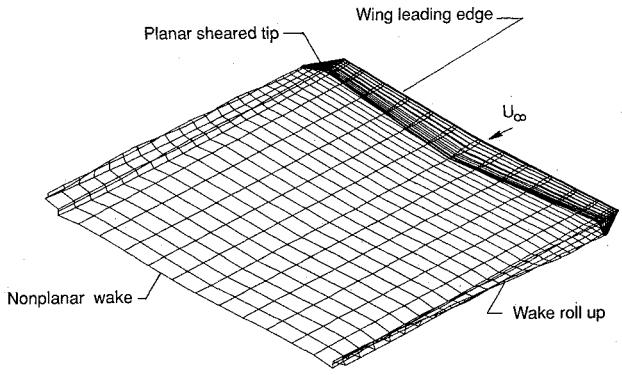

Fig. 1 Surface-panel representation and wake shape of wing with 60-deg sheared tips at cruise condition.

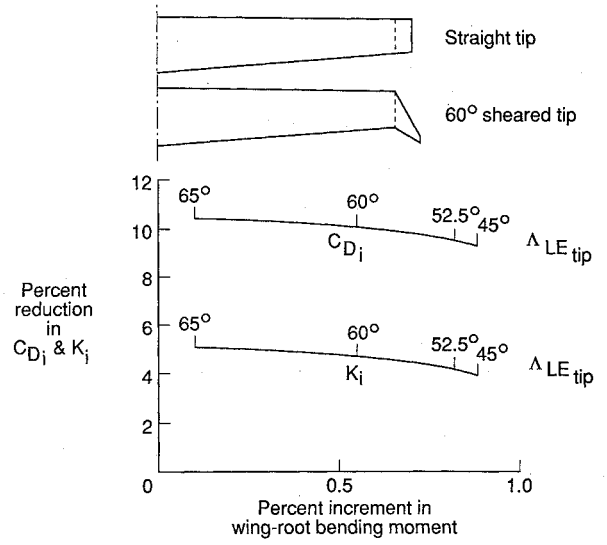

Fig. 2 Effect of wing-tip leading-edge sweep angle ($\Lambda_{LE_{tip}}$) on induced drag and wing-root bending moment at $C_L = 0.4$.

typical wing with sheared tips and its wake. (Note that the number of panels in the figure is reduced for the purpose of clarity.) Lift coefficient C_L and drag coefficient C_D ($= C_{D_i}$ for an inviscid panel method) are calculated by integrating the surface pressure coefficients and dividing by the reference area. The calculations are performed for sufficiently dense panel distributions to allow accurate integration of the surface pressures.[9]

Results are presented herein for a tapered, high-aspect-ratio, unswept, untwisted wing with several different sheared-tip configurations (see Fig. 2). Several sheared-tip configurations were analyzed to determine the effects of increased tip leading-edge sweep angle ($\Lambda_{LE_{tip}}$) on spanwise load distribution and induced drag of the wing. The proposed tip configurations are similar to those originally described by van Dam.[16] Only the outboard 7.3% of the semispan of the baseline wing was modified while a constant planform area was maintained. The baseline tip shape used in this design study was a rectangular tip derived from the taper characteristics of the inboard planform (Fig. 2). Although total wing area was constant for all wing configurations, wing span varied slightly. In Fig. 2, the predicted effects of the sheared wing tips on induced-drag coefficient C_{D_i}, induced-drag factor K_i, and wing-root-bending moment coefficient *WRBM* are presented for a cruise $C_L = 0.40$. The computed changes are in comparison to the wing with the baseline tips.

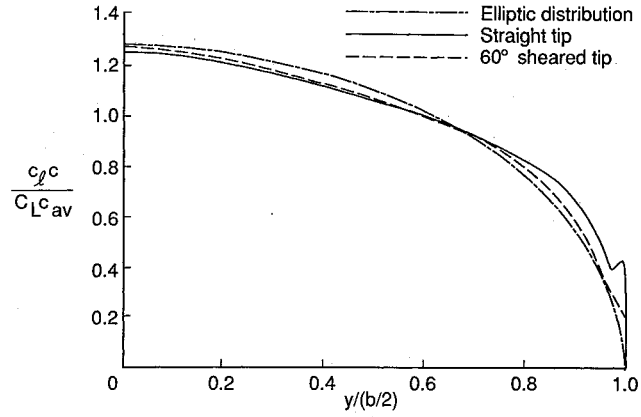

Fig. 3 Calculated spanwise load distributions for baseline wing and wing with 60-deg sheared tip at $C_L = 0.4$.

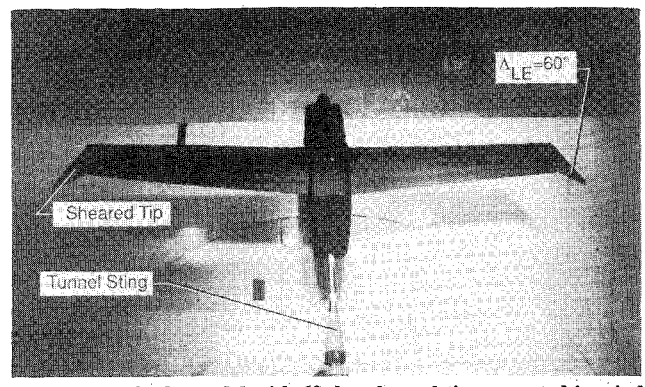

Fig. 4 Wing-body model with 60-deg sheared tips mounted in wind tunnel.

The induced-drag coefficient can be written as follows:

$$C_{D_i} = K_i(C_L^2/\pi \mathcal{R}) \tag{1}$$

where K_i can be greater or smaller than unity, and $\mathcal{R} = b^2/S$ represents wing aspect ratio. For $K_i = 1.0$, Eq. (1) represents the classical minimum induced-drag coefficient for an unswept planar wing with an elliptic spanwise load distribution. The predicted reduction in C_{D_i}, as shown in Fig. 2, is caused by both the increase in span and the improved efficiency of the wing with sheared tips. These two effects are separated in the analysis by accounting for the change in aspect ratio. Consequently, the reduction in K_i is a direct measure of the improvement in aerodynamic efficiency. Figure 2 shows that, as the leading-edge sweep angle of the sheared tips increases, the wing becomes more efficient. A reduction in C_{D_i} of 10.5% is predicted for the 65-deg tips, and the reduction in K_i is 4.8% in comparison to the baseline configuration.

The spanwise load distributions for the baseline and the 60-deg configurations are compared with the elliptic distribution in Fig. 3. Note a slight shift of the spanwise loading toward the inboard portion of the wing as a result of the tip modification. Consequently, the bending moment at the wing root is hardly affected by the change in tip shape. An increase in *WRBM* of about 0.5% is calculated for the 60-deg configuration. Also, note the improvement in the local load distribution near the wing tip; specifically, the bump in the load distribution of the baseline wing is eliminated with the sheared tip. The bump in the tip loading is not predicted by linear computational methods.[16] Wake relaxation is essential to correctly predict the load distribution near the tip and, thus, to study the effect of wing-tip geometry on induced drag.

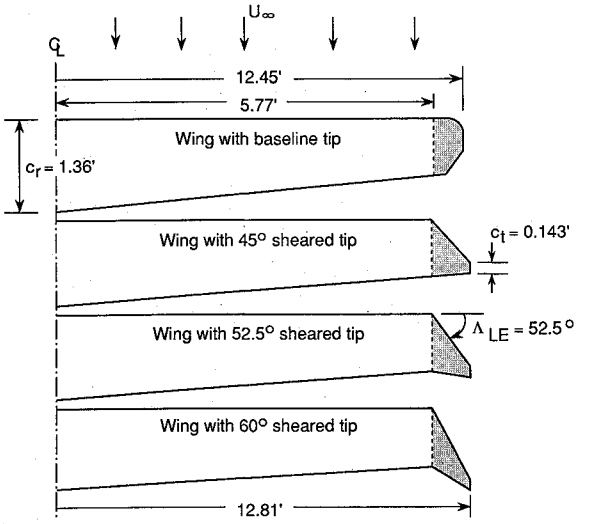

Fig. 5 Planform geometry of wing and tips investigated in experiment.

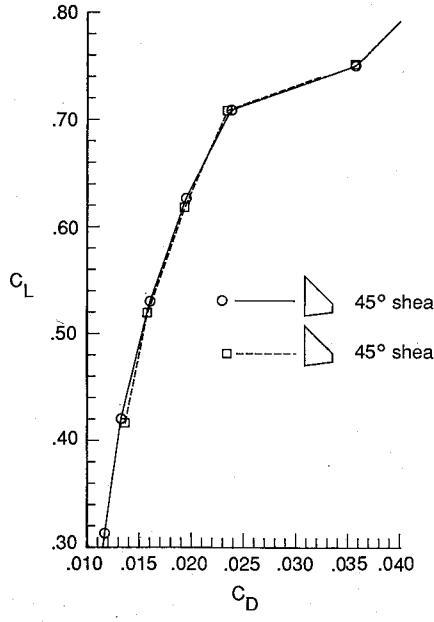

Fig. 6 Repatability of drag data for $q = 30$ lb/ft^2 and $(x/c)_{tr} = 0.60$.

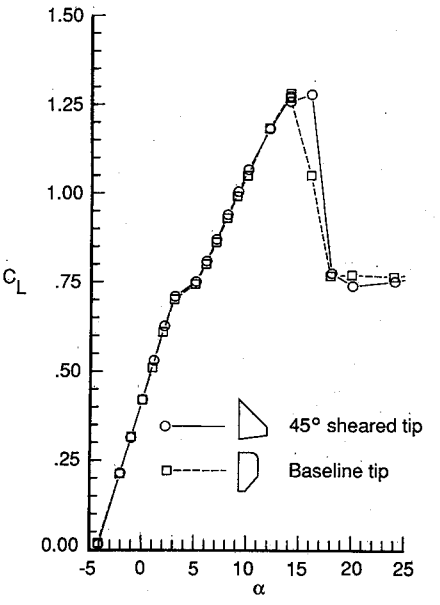

a) Lift curves

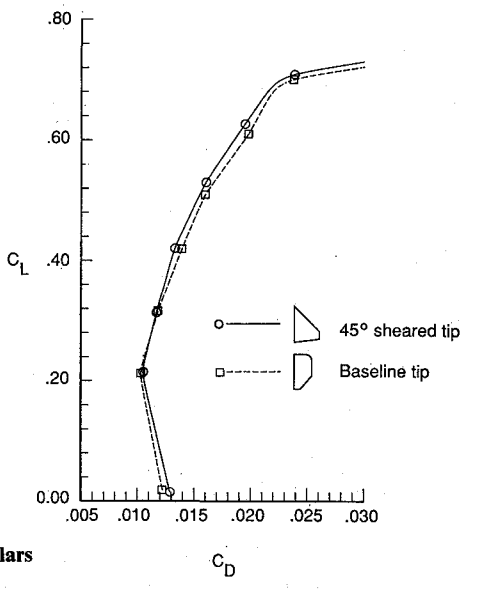

b) Drag polars

Fig. 7 Measured lift curves and drag polars for baseline and 45-deg sheared-tip configuration; $(x/c)_{tr} = 0.60$.

Wind-Tunnel Experiment

A wind-tunnel investigation of the effects of the sheared wing tips was conducted in the 14 × 22-ft Subsonic Tunnel at NASA Langley Research Center. The objectives of the experiment were to confirm the computed reductions in induced drag produced by the sheared wing tips and to examine the static-stability and the high-angle-of-attack characteristics of a wing with sheared tips. Figure 4 shows a photograph of the model with 60-deg sheared tips in the wind tunnel. This wind-tunnel model with high-aspect-ratio wing happened to be available and resembles an actual airplane configuration that may be used to test these types of tip shapes in flight. The four tested wing configurations are sketched in Fig. 5. All configurations had identical wing area (S_{ref} = 13.06 ft^2) and identical shape inboard from wing semispan station $y = \pm 5.77$ ft. The baseline wing had an aspect ratio $AR = 11.86$, whereas the modified wings had an aspect ratio $AR = 12.56$, i.e., an increase of 5.9% as compared to the baseline wing. The section shape of the wing and the sheared tip in the freestream direction was the NASA NLF(1)-0414F airfoil.[18] The baseline wing tip available in the experiment was shaped slightly differently from the baseline tip used in the design study. The experimental baseline tip was based on the work by Nicks.[17]

The majority of the test data presented in this paper were obtained at a freestream dynamic pressure $q = 30$ lb/ft^2 (model strength limitations precluded a higher q) and a unit Reynolds number of about 1.0×10^6 ft^{-1}. The dynamic pressure was reduced to 25 lb/ft^2 for angle of attack $\alpha = 14$ and 16 deg to avoid excessive dynamic rolling loads on the balance due to buffet at these wing-stall angles of attack. Both the maximum lift capability of the model and the angle of attack for which the maximum lift was attained were not affected by the small reduction in Reynolds number.

Boundary-layer transition was fixed at 60% of the chord on the upper and lower surface along the entire wing span. This chordwise location corresponded approximately with the onset of pressure recovery for design (cruise) lift coefficients.[18] Use of transition grit at this location eliminated potential separation of the laminar boundary layer. In addition, selected measurements were made with transition grit near the leading edge

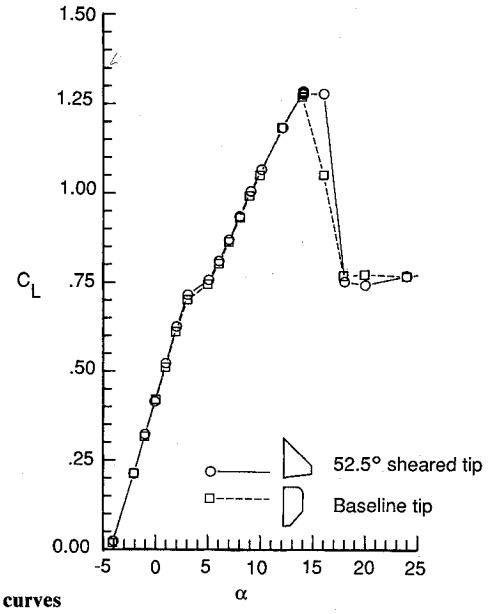

a) Lift curves

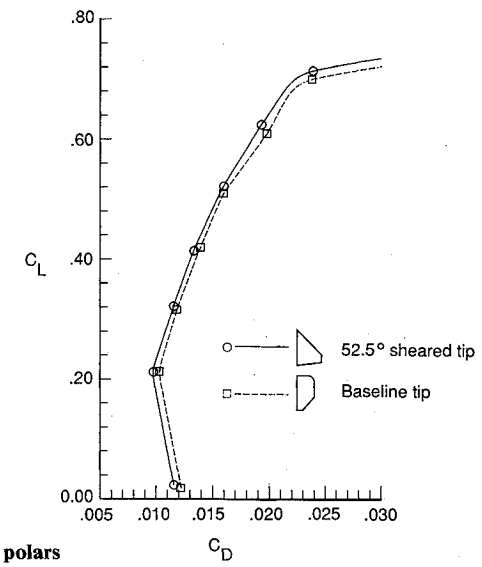

b) Drag polars

Fig. 8 Measured lift curves and drag polars for baseline and 52.5-deg sheared-tip configuration; $(x/c)_{tr} = 0.60$.

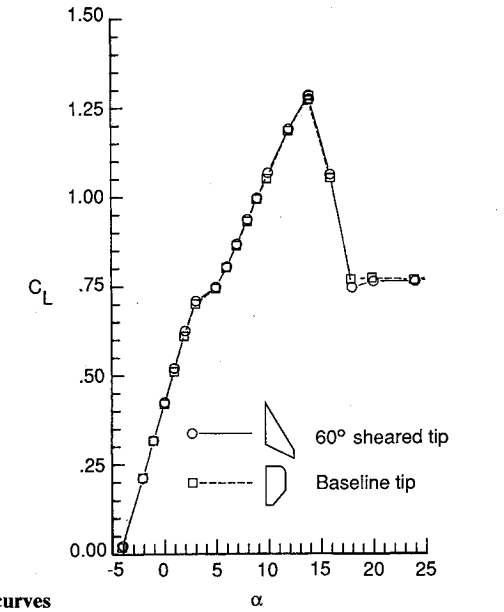

a) Lift curves

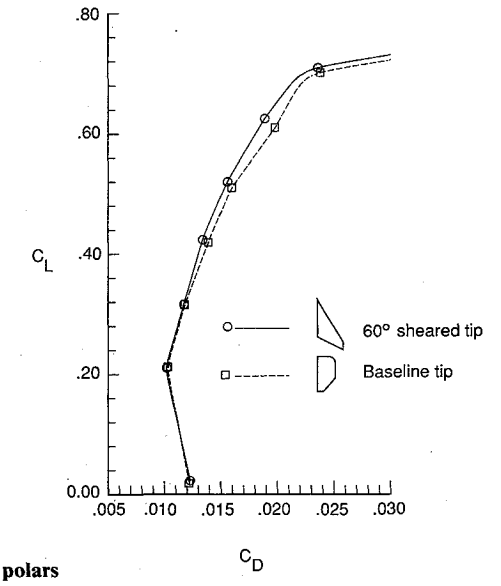

b) Drag polars

Fig. 9 Measured lift curves and drag polars for baseline and 60-deg sheared-tip configuration; $(x/c)_{tr} = 0.60$.

at the 5% wing chord location in lieu of the 60% location. On the centerbody the transition location was fixed circumferentially at 10% of the body length. For each model configuration forces and moments were measured for an angle-of-attack range from −5 to 40 deg at zero sideslip angle. Also, force and moment measurements were made for an angle-of-sideslip range from −10 to 10 deg at several angles of attack.

Wind-off tares were carefully determined after each change in configuration. At each angle of attack, balance readings were taken over a period of 10 s at a rate of 5 readings/s. In the following figures, each experimental data point represents the average value of these readings. In Fig. 6, lift and drag results are compared for a typical sheared-tip configuration over the most pertinent angle-of-attack range. The comparison of the data between the two runs shows that the repeatability of the drag data was better than five drag counts.

Experimental Results and Discussion

In this section, measured lift-and-drag and static-stability characteristics for the model with the four tip configurations are presented. Also, the calculated lift and drag of the tested wing-body configurations are compared to the measured values. The moments are presented with respect to a fixed point on the model centerline, located longitudinally at the 0.25 $\bar{c}$ location of the baseline wing (0.275 ft aft of the leading edge), and located vertically at 0.075 ft below the 0.25 $\bar{c}$ point (where $\bar{c}$ is the mean aerodynamic chord). The lateral-directional moments are referred to the body-axis system with the origin located at the moment center. The aerodynamic coefficients were reduced by the reference wing area of 13.06 ft^2, the reference wing span of 12.00 ft, and the reference chord $\bar{c}$ of 1.10 ft.

Lift and Drag Characteristics

In Figs. 7–9, the measured lift curves and drag polars for the three sheared-tip configurations are presented and compared with the results for the baseline configuration. The lift curves for the various models are shown in Figs. 7a, 8a, and 9a. Around $\alpha = 5$ deg ($C_L \simeq 0.75$), boundary-layer transition location on the upper surface of the wing shifted from the grit location at 60% of the chord to the leading-edge region as a result of the leading-edge suction peak. The forward shift of transition location resulted in premature separation of the tur-

bulent boundary layer near the trailing edge. This produced a loss in lift for a constant angle of attack and, consequently, a reduction in lift curve slope C_{L_α} of about 30%. The premature separation can be attributed to the off-design operation of the natural-laminar-flow airfoil in terms of Reynolds number. In the present test, the Reynolds number based on the mean aerodynamic chord $\bar{c}$ was 1.1×10^6, approximately an order of magnitude less than the design Reynolds number of the airfoil section.[18] The configurations with the sheared tips exhibited lift characteristics very similar to the baseline model. Maximum lift was observed to occur near $\alpha = 15$ deg and $C_{L_{max}} = 1.30$ for all configurations. The stall characteristics of the modified wings were very similar to those of the wing with the baseline tips at these test conditions.

The drag polars for the lift range of interest are shown in Figs. 7b, 8b, and 9b. The previously discussed rapid forward movement of the transition location on the upper surface of the entire wing at $C_L \simeq 0.75$ caused the substantial increase in drag observed for all configurations. A reduction in drag over most of the lift range was measured for the sheared tips when compared with the baseline configuration. In contrast to nonplanar tip devices, such as winglets, the sheared tip did not produce a "crossover" behavior in lift coefficient below which a drag penalty is incurred due to the increase in wetted area.[19]

Generally, induced-drag characteristics can be studied in more detail by examining the linearized drag polar, i.e., C_D vs C_L^2. In Fig. 10, the results for all four configurations tested are depicted for the most pertinent angle of attack range. For $0.04 \le C_L^2 \le 0.40$, the curves in Fig. 10 are approximately linear. The drag polar for an untwisted wing may be written as the sum of profile drag and induced drag, or

$$C_D = C_{D_{min}}^* + K_P(C_L - C_{L_{min}}^*)^2 + K_i(C_L^2/\pi AR) \qquad (2)$$

where $C_{D_{min}}^*$ is the minimum profile drag coefficient, K_P is the profile-drag factor, and $C_{L_{min}}^*$ is the lift coefficient for minimum profile drag. When the total drag coefficient C_D is differentiated with respect to $C_{L_{min}}^2$, the following expression is obtained:

$$\frac{dC_D}{dC_L^2} = K_P\left(1 - \frac{C_{L_{min}}^*}{C_L}\right) + \frac{K_i}{\pi AR} \qquad (3)$$

Notice that the slope of the linearized drag polar in this form is a function of C_L unless $K_P = 0$ or $C_L = C_{L_{min}}^*$. For the NLF(1)-0414F wing section, K_P is approximately zero for lift conditions inside the drag bucket, and $C_{L_{min}}^* \simeq 0.40$.[18] For $0.04 \le C_L^2 \le 0.40$, the wing operates inside the drag bucket, and the deviations from $C_{L_{min}}^*$ are rather small; thus, $K_i \simeq \pi AR/(dC_L^2/dC_D)$. [Another approach to determine K_i from the experimental data would be to plot C_D vs $(C_L - C_{L_{min}})^2$, where $C_{L_{min}}$ represents the lift coefficient for minimum total drag coefficient $C_{D_{min}}$. In this case

$$\frac{dC_D}{d(C_L - C_{L_{min}})^2} = K_P + K_i/(\pi AR)$$

which is independent of C_L. However, the problem with this approach is that it requires an accurate experimental value for $C_{L_{min}}$.] The slope $\Delta C_L^2/\Delta C_D$ for all three sheared-tip configurations is steeper than that of the baseline, indicating a reduction in induced drag. Although the curves in Fig. 10 are approximately linear, the number of data points in the pertinent C_L^2 range precludes an accurate determination of K_i using Eq. (3).

The benefits of the sheared tips can more clearly be depicted by comparing the lift-to-drag ratios as a function of C_L (see Fig. 11). Maximum lift-to-drag ratio $(L/D)_{max}$ occurred at $C_L \simeq 0.50$, and the largest measured improvement in $(L/D)_{max}$ was 4.6% for the 60-deg configuration. This improvement in $(L/D)_{max}$ corresponds to a net reduction in K_i of 3.3% when one takes into account the difference in aspect ratio and assumes a parabolic drag polar [Eq. (2)], with $C_{D_{min}}^*$ unchanged and $K_P = 0$. Similarly, based on the increment in measured $(L/D)_{max}$, K_i improved by about 1.6% for the 45-deg tip and decreased by 1.0% for the 52.5-deg wing tip. These measured improvements in aerodynamic efficiency based on the increase in $(L/D)_{max}$ are in good agreement with the improvements based on the increase in slope $\Delta C_L^2/\Delta C_D$ of the linearized drag polar. Although the experimental trends in induced-drag reduction with sweep angle correlate fairly well with the predicted benefits (Fig. 2), the experimental values fall below the calculated values. The source of the discrepancy is the difference between the computational (Fig. 2) and the experimental (Fig. 5) baseline tip shape. The baseline tip shape used in the wind-tunnel test was modeled, and it produced an improvement in K_i of 2.2% as compared to the baseline tip used in the computational design. As a result, the computed and measured drag improvements due to the sheared tips are in fair agreement. In addition, it demonstrates the strong influence of the outboard wing portion on induced drag and the good results that can be obtained with current aerodynamic codes such as VSAERO.

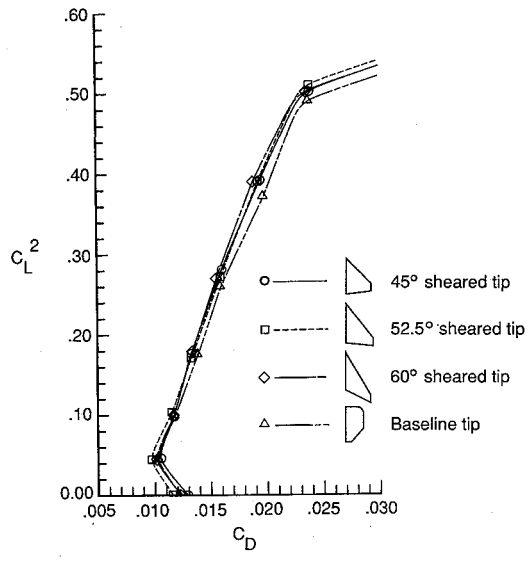

Fig. 10 Linearized drag polars for baseline and sheared-tip configurations; $(x/c)_{tr} = 0.60$.

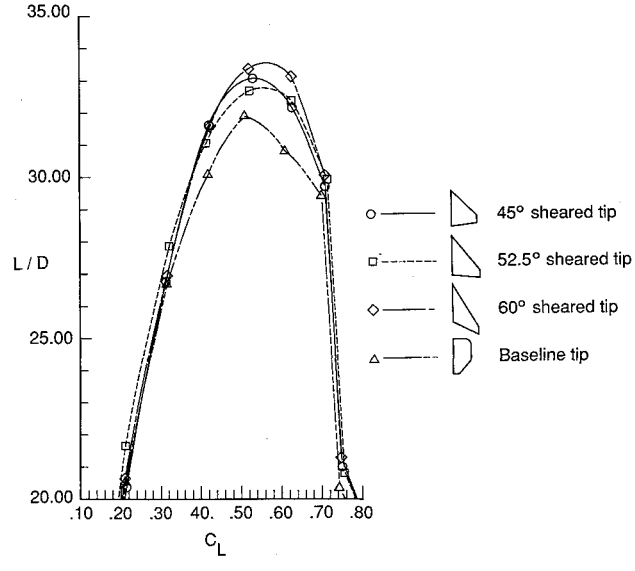

Fig. 11 Lift-to-drag ratios for baseline and sheared-tip configurations; $(x/c)_{tr} = 0.60$.

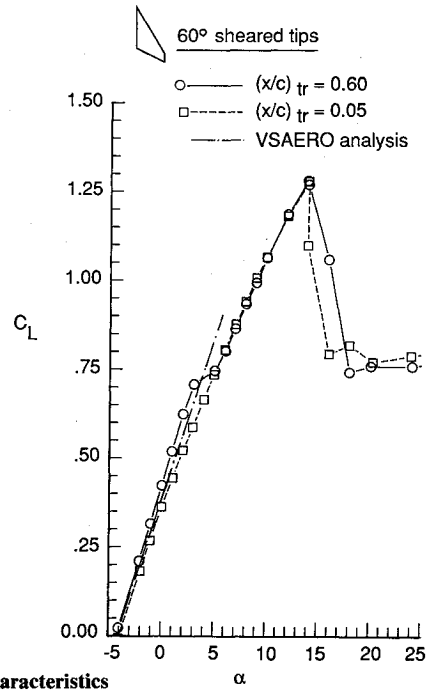

a) Lift characteristics

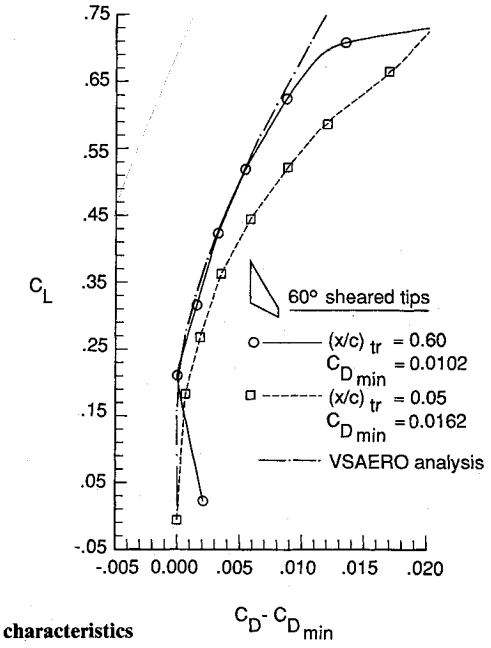

b) Drag characteristics

Fig. 12 Comparison of calculated and measured lift and drag characteristics for model with 60-deg sheared tips.

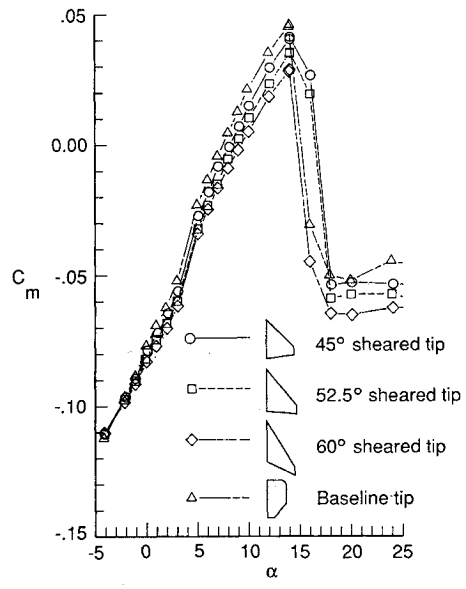

Fig. 13 Effect of wing-tip configuration on longitudinal static stability characteristics; $(x/c)_{tr} = 0.60$.

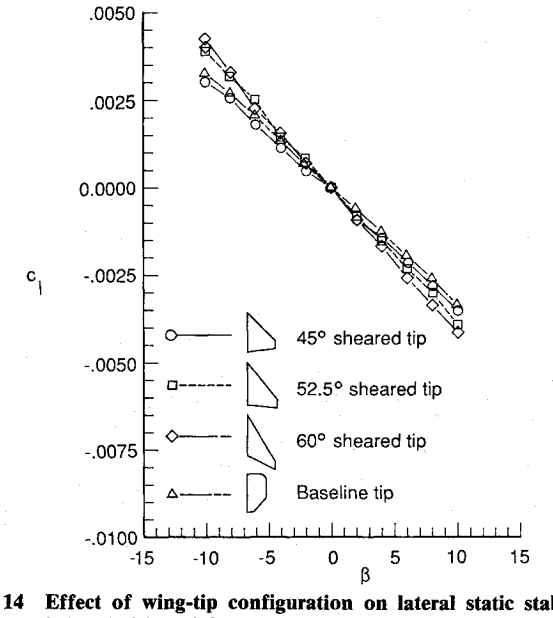

Fig. 14 Effect of wing-tip configuration on lateral static stability characteristics; $(x/c)_{tr} = 0.05$ and $\alpha = 0$ deg.

In Fig. 12, experimental data are compared with calculated results for the fuselage-wing configuration with 60-deg sheared tips. A total of 1000 panels were used to model the configuration, including 120 panels for the fuselage. With transition fixed near the leading edge, the decambering effect of the turbulent and partially separated boundary layer on C_{L_α} can be clearly observed in Fig. 12a. For $\alpha > 5$ deg, both experimental curves are in good agreement because in both tests transition occurred near the leading edge independent of the location of the trip strip. The predicted lift curve is in fair agreement with the wind-tunnel results. As indicated earlier, the calculations do not include viscous effects. In order to facilitate a comparison between calculated and measured drag data, the measured value for $C_{D_{min}}$ was subtracted from the measured drag values, as shown in Fig. 12b. A large increment in $C_{D_{min}}$ was measured when transition was forced near the leading edge of the wing; $C_{D_{min}}$ increased from 102 to 162 drag counts. Good agreement was obtained between the calculated and measured drag polars for C_L up to 0.65 when transition was fixed at 60% of the chord, the lift range for which the form drag contribution is very small. However, notice the large form drag contribution with lift coefficient when transition occurred near the leading edge.

Longitudinal and Lateral-Directional Characteristics

In Fig. 13 the longitudinal static-stability characteristics of the wind-tunnel models are presented. Rearward sweep of the wing tips resulted in a rearward shift of the aerodynamic center of the wing and thus a reduction in longitudinal instability for the (tail-off) wing-body model. For the model with the 60-deg tips, the pitching-moment-curve-slope C_{m_α} was reduced by about 12%, as compared to C_{m_α} for the baseline tips. At angles of attack near stall ($\alpha \simeq 14$ deg), this change in slope resulted in a reduction in pitch-up moment by about 40% for the 60-deg configuration.

The lateral-directional static-stability characteristics were measured by varying sideslip angle β for a constant angle of attack. In Fig. 14 the variation in rolling-moment coefficient C_l is shown for $\alpha = 0$ deg, with transition fixed at $x/c = 0.05$. A pronounced increase in lateral static stability was obtained with increasing tip sweep angle. For the 45-deg tip the increment in dihedral effect was relatively small; however, dihedral effect was increased by as much as 20% for the 60-deg tip. Similar changes in lateral stability were observed at higher angles of attack ($\alpha = 8$ and 12 deg). The effect of the sheared tips on the directional static stability of the model was negligible for all the angles of attack tested.

Concluding Remarks

A series of sheared wing tips was evaluated theoretically and experimentally for effects on performance and static stability of an unswept, untwisted, high-aspect-ratio wing. The theoretical analysis was performed using a nonlinear surface-panel method to include the effects of the nonplanar wake on the aerodynamic forces and moments. A wind-tunnel experiment was conducted using a high-aspect-ratio unswept wing to verify the predicted induced-drag reductions due to the sheared tips. The leading-edge sweep angles of the straight sheared tips tested in the wind tunnel were 45, 52.5, and 60 deg. The test was conducted in the NASA Langley 14 × 22-ft Subsonic Tunnel with a 12-ft span wing-body model.

The wind-tunnel data showed that longitudinal and lateral static stability increased with increasing tip leading-edge sweep angle, whereas directional static stability remained unchanged. Longitudinal static stability improved by 12%, and dihedral effect increased by as much as 20% for the 60-deg sheared tip in comparison to the (unsheared) baseline configuration. Also, model lift characteristics, including stalling behavior, were largely unaffected by the changes in tip configuration at the test Reynolds number of about 10^6.

The main emphasis of this study was on the potential induced-drag reduction as a result of the application of sheared tips. The wind-tunnel measurements showed an increase in $(L/D)_{max}$ of 4.6% for the 60-deg sheared wing-tip configuration. This translates into a net increase in aerodynamic efficiency of about 3.3% due to sheared tips. The trend in, and the magnitude of, the measured reduction in induced drag with tip leading-edge sweep angle agrees fairly well with the predicted effects of sheared tips. The calculations and the measurements demonstrate the strong influence of sheared-tip geometry on induced drag.

References

[1]Hemke, P. E., "Drag of Wings with End Plates," NACA Rept. 267, 1927.

[2]Mangler, W., "The Lift Distribution of Wings with End Plates," NACA TM 856, 1938.

[3]Whitcomb, R. T., "Design Approach and Selected Wind Tunnel Results at High Subsonic Speeds for Wing-Tip Mounted Winglets," NASA TN D-8260, July 1976.

[4]Pfenninger, W., "Design Considerations of Large Global Range High Subsonic Speed LFC Transport Airplanes," *Special Course on Concepts for Drag Reduction,* AGARD Rept. 654, June 1977, pp. 3-63–3-75.

[5]Spillman, J. J., "The Use of Wing-Tip Sails to Reduce Vortex Drag," *Aeronautical Journal,* Sept. 1978, pp. 387–395.

[6]Hackett, J. E., "Vortex Drag Reduction by Aft-Mounted Diffusing Vanes," International Council of the Aeronautical Sciences, Paper 80-13.4, Oct. 1980, p. 542.

[7]Zimmer, H., "The Aerodynamic Optimization of Wings in Subsonic Speed Range and the Influence of the Design of the Wing Tips," Dr. Ing, Dissertation, Univ. of Stuttgart, Stuttgart, FRG, June 1983 (in German).

[8]van Dam, C. P., "Efficiency Characteristics of Crescent Shaped Wings and Caudal Fins," *Nature,* Vol. 325, Jan. 1987, pp. 435–437.

[9]van Dam, C. P., "Induced-Drag Characteristics of Crescent-Moon-Shaped Wings," *Journal of Aircraft,* Vol. 24, Feb. 1987, pp. 115–119.

[10]Prandtl, L., "Applications of Modern Hydrodynamics to Aeronautics," NACA Rept. 116, 1921.

[11]Munk, M. M., "The Minimum Induced Drag of Aerofoils," NACA Rept. 121, 1921.

[12]Maskell, E. C., "Progress Towards a Method for the Measurement of the Components of the Drag of a Wing of Finite Span," Royal Aeronautical Establishment, TR 72232, Dec. 1972.

[13]Sears, W. R., "On Calculation of Induced Drag and Conditions Downstream of a Lifting Wing," *Journal of Aircraft,* Vol. 11, March 1974, pp. 191–193.

[14]Weston, R. P., "Refinement of a Method for Determining the Induced and Profile Drag of a Finite Wing from Detailed Wake Measurements," Ph.D. Dissertation, Univ. of Florida, Gainesville, FL, 1981.

[15]Maskew, B., "Prediction of Subsonic Aerodynamic Characteristics—A Case for Low-Order Panel Methods," *Journal of Aircraft,* Vol. 19, Feb. 1982, pp. 157–163.

[16]van Dam, C. P., "Swept Wing-Tip Shapes for Low-Speed Airplanes," Society of Automotive Engineers, Paper 85-1770, Oct. 1985; also *SAE Transactions,* Vol. 96, 1986, pp. 355–363.

[17]Nicks, O. W., "Wing Extensions for Improving Climb Performance," AIAA Paper 83-2556, Nov. 1983.

[18]McGhee, R. J., Viken, J. K., Pfenninger, W., Beasley, W. D., and Harvey, W. D., "Experimental Results for a Flapped NLF Airfoil with High Lift/Drag Ratio," NASA TM 85788, May 1984.

[19]van Dam, C. P., Holmes, B. J., and Pitts, C., "Effect of Winglets on Performance and Handling Characteristics of General Aviation Aircraft," *Journal of Aircraft,* Vol. 18, July 1981, pp. 587–591.